https://doi.org/10.5194/essd-2026-437
Preprint. Discussion started: 11 August 2026

Open Access Earth System Science Data Discussions

A dataset of soil water measurements at multiple scales and depths on China's Loess Plateau

Wen Zhao[1,2], Xiaoxu Jia[1,2,7*], Wei Hu[3], Xuezhang Li[4], Chunlei Zhao[1,2], Lei Gao[5], Yuhua Jia[6], and Ming'an Shao[1,2,7]

[1]Institute of Geographic Sciences and Natural Resources Research, Chinese Academy of Sciences, Beijing 100101, China

[2]College of Resources and Environment, University of Chinese Academy of Sciences, Beijing 100190, China

[3]Bioeconomy Science Institute, Private Bag 4704, Christchurch 8140, New Zealand

[4]Institute of Subtropical Agriculture, Chinese Academy of Sciences, Changsha 410125, China

[5]Institute of Soil Science, Chinese Academy of Sciences, Nanjing 210008, China

[6]College of Water Conservancy, Shenyang Agricultural University, Shenyang 110866, China

[7]State Key Laboratory of Soil Erosion and Dryland Farming on the Loess Plateau, Northwest A&F University, Yangling, Shaanxi 712100, China

Correspondence: Xiaoxu Jia (jiaxx@igsnrr.ac.cn)

https://doi.org/10.5194/essd-2026-437
Preprint. Discussion started: 11 August 2026

Open Access Earth System Science Data Discussions

Abstract. Soil water content (SWC) is a key state variable in land-surface hydrological processes and the primary water source for vegetation, particularly in arid and semi-arid regions. However, long-term, multi-scale in situ measurements of deep SWC remain insufficient on the Loess Plateau of China (LPC), the world's largest and deepest loess deposit area. To address this gap, the Loess-Obs network, a long-term multi-scale SWC observation system, was established on the LPC about 20 years ago, covering five spatial scales including plot, hillslope, local-landscape, plateau-wide transect, and regional-survey scale. Here, we present a long-term SWC profile dataset derived from the Loess-Obs network, including continuous measurements (2004–2019) of four plots with distinct land uses, two hillslope transects of 300 m and 270 m (2004–2016), a 1340 m local-landscape transect spanning multiple hillslopes (2012–2013), an 860 km plateau-wide transect (2013–2016), and a regional survey conducted in 2015. Volumetric SWC in the 0–5 m layer was measured at multiple depths using calibrated neutron probes (sampling frequency: weekly to monthly). We detail the network design, field protocols, experimental setup, sampling strategies, calibration equations, maintenance procedures, and quality control measures, alongside associated environmental datasets (land use, soil properties, topography, meteorology) to support extended applications. Key findings include: (1) exotic shrubs (*Caragana korshinskii*) and grasses (*Medicago sativa*) accelerated deep SWC depletion compared to cropland and naturally restored fallow land; (2) temporal variability of SWC decreased, while its spatial variability increased with soil depth; (3) time-stable sampling sites could be effectively used to characterize mean SWC of different soil layers, with accuracy improving with depth; (4) regional soil water storage decreased from southeast to northwest; (5) the discrepancy between SWC products and Loess-Obs observations generally increased with depth, reflecting the scarcity of deep *in situ* observations in model development. This dataset is valuable for validating SWC products, developing upscaling methods, and understanding deep soil hydrological responses to land use and climate change. It is publicly accessible at https://zenodo.org/records/21859310.

https://doi.org/10.5194/essd-2026-437
Preprint. Discussion started: 11 August 2026

1 Introduction

Soil water is a critical component of the soil-plant-atmosphere continuum and drives geophysical and biogeochemical processes in the Earth's critical zone (Kirkby, 2016; Cooper et al., 2021; Jia et al., 2024). Quantifying the spatiotemporal variations and trends of soil water content (SWC) is essential for understanding hydrological and vegetation responses to climate change, particularly in arid and semi-arid regions (Huang and Shao, 2019). Over the past few decades, global SWC data have been acquired via *in situ* measurements, remote sensing, and model simulations (Rodell et al., 2004; Entekhabi et al., 2010; Babaeian et al., 2019; Tavakol et al., 2021), supporting applications such as terrestrial water cycle analysis and soil-plant-water relation research (Crow et al., 2012). Among these, *in situ* measurements are fundamental for calibrating and validating remote sensing and model products, and improving model parameterization (Mertens et al., 2005; Duan et al., 2019; Beck et al., 2021).

The Loess Plateau of China (LPC) is globally unique for its severe soil erosion and extensive loess deposits, with two-thirds of the area classified as arid or semi-arid (Jia et al., 2024). In this water-scarce region with deep groundwater tables, SWC is the primary limiting factor for plant growth and ecosystem sustainability (Jia et al., 2017a), making it a key parameter for water resource management and vegetation restoration. Despite numerous studies of SWC on the LPC, including responses to vegetation restoration (Jian et al., 2015; Liu and Shao, 2015; Li et al., 2021), multi-scale variability (Gao et al., 2011; Yang et al., 2012; Yu et al., 2018), scale effects on hydrological modeling (Biswas et al., 2013; Li et al., 2019), and soil desiccation (Jia et al., 2020), existing datasets have following critical limitations: remote-sensing data products cannot adequately capture deep SWC (Peng et al., 2021), single-site measurements lack spatial representativeness, and most observations are restricted to shallow soils (Rao et al., 2022), single land uses (Xu, 2018), or limited spatiotemporal coverage (Wang et al., 2019). A comprehensive dataset reflecting deep SWC multi-scale variations and long-term land use impacts is urgently needed.

https://doi.org/10.5194/essd-2026-437
Preprint. Discussion started: 11 August 2026

To fill this gap, Loess-Obs network, the first operational SWC observatory on the LPC, was established in 2004 to provide representative coverage of diverse land uses and spatial scales. Using non-destructive neutron probe technology (Zreda et al., 2008; Desilets et al., 2010; Kodikara et al., 2014), Loess-Obs enables repeated deep SWC measurements (3–5 m) across plot, hillslope, local-landscape, plateau-wide transect, and regional-survey scales. Here, we present the long-term (2004–2019) Loess-Obs dataset, including SWC measurements, soil properties, and environmental covariates. Our objectives are to: (1) describe the dataset generation and validation; (2) examine long-term land use effects on SWC; and (3) analyze spatiotemporal variability of SWC across scales.

2 Study area

The LPC is located in the upper-middle reaches of the Yellow River (33°41′ N–41°16′ N, 100°52′ E–114°33′ E), covering an area of approximately 64×10^4 km^2 (Huang and Shao, 2019; Zhu et al., 2019). The Loess-Obs network spans the typical loess region of the LPC (approximately 37×10^4 km^2; Fig. 1) and is characterized by a warm-temperate continental monsoon climate. Mean annual precipitation ranges from 150 to 800 mm (zonal transition from arid to semi-humid), with 70–80% falling as high-intensity rainstorms in July-September; mean annual temperature increases from 3.6 °C (northwest) to 14.3 °C (southeast); and evaporation ranges from 1000 to 2000 mm (exceeding 3000 mm in some areas).

Notably, the LPC is the world's largest loess deposit, with thickness ranging from 0 to 350 m (mean: 92.2 m excluding mountains; Zhu et al., 2018). Soils are loess-derived, with sandy textures in the northwest and clayey textures in the southeast. Typical landforms include loess Yuan (flat surfaces), Liang (long ridges), Mao (round hills), and valleys or gullies (Yang et al., 2009), with terraces widely constructed to mitigate soil erosion and create agricultural fields. Furthermore, natural vegetation transitions from forest to desert steppe from southeast to northwest. Historical cropland expansion has caused severe soil erosion and land degradation. To control soil erosion and improve the ecological environment, large-scale vegetation restoration has been widely implemented on the LPC (e.g., the 1999 Grain-for-Green Project),

https://doi.org/10.5194/essd-2026-437
Preprint. Discussion started: 11 August 2026

which increased vegetation cover from 31.6% in 1999 to 64.2% in 2021 (Chen et al., 2024). Dominant crops include winter wheat, maize, soybeans, millet, and potatoes, while exotic planted species include black locust, Chinese pine, korshinsk peashrub, sea buckthorn, and alfalfa.

3 Data and methodology

3.1 Loess-Obs network and *in situ* SWC profile measurements

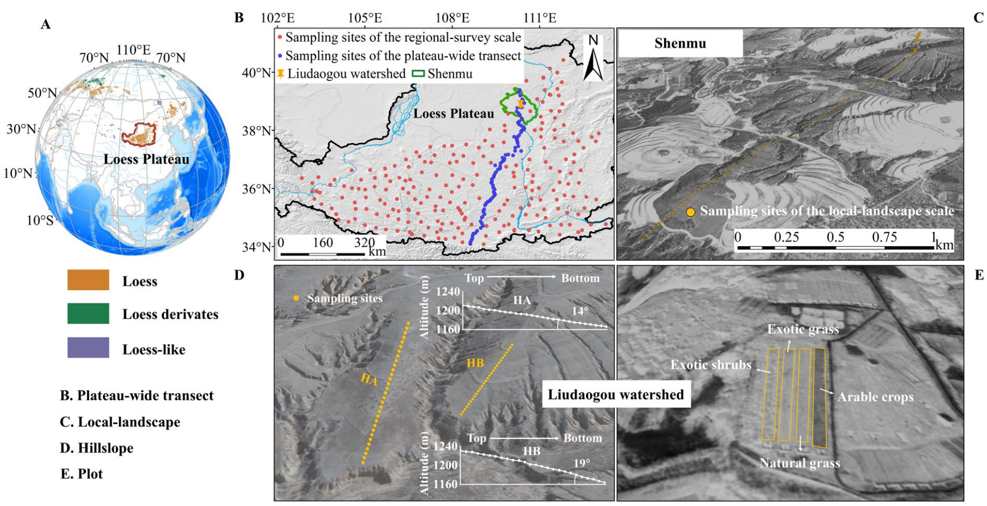

Figure 1 Distribution of sampling points at different spatial scales. A shows the global distribution of loess and the location of the LPC; B shows the sampling points at the regional-survey scale (red points) and along a plateau-wide transect running broadly north-south (blue points) on the Loess Plateau; C shows the sampling points along a local-landscape transect; D shows the sampling points on the hillslope A (HA) and the hillslope B (HB); and E shows the four long-term plots.

Loess-Obs was initially established in 2004 and includes five SWC monitoring scales: plot, hillslope, local-landscape, plateau-wide transect, and regional-survey. Each scale comprises multiple *in situ* SWC monitoring sites, with each site equipped with an aluminum neutron-probe access tube (3.2–5.2 m in length). SWC measurements were conducted using neutron probes during the growing seasons (April to October) each year. Volumetric SWC at each depth was calculated from slow-neutron counting rates using scale-specific calibration curves (Table 1). The neutron probe technology indirectly estimates SWC by measuring the slowing rate of neutron intensity due to collisions with molecular hydrogen in soil water, offering non-destructive, rapid measurements suitable for various soil types and frozen conditions (Kodikara et al., 2014).

3.1.1 Regional-survey scale

The spatial distribution of SWC at the regional-survey scale was investigated using a grid sampling approach with a 40 km interval in the typical loess region of the LPC. In areas with complex landscapes and geomorphology, the sampling interval was reduced to less than 40 km to ensure representativeness. At least one sampling points was selected per grid cell, considering road accessibility and the representativeness of geomorphology, land use, soil type, and vegetation type. Field soil sampling was conducted at least 200 m away from roads and villages to minimize anthropogenic interference.

A total of 243 sampling points (46 farmlands, 95 forestlands, 14 shrublands, 88 grasslands) were surveyed across the typical loess region during June–October 2013 (Fig. 1). At each point, a 5.2 m deep aluminum neutron probe access tube was installed to measure volumetric SWC (0–5.0 m) at 0.2 m intervals between May and June 2015 using a CNC 503DR Hydro probe (Beijing Super Power Company, Beijing, China), resulting in 6,075 measurements. The neutron probe used a 50 millicurie americium-beryllium source with a 64 s counting time per measurement. A polyethylene surface tray (0.3 m diameter, 0.04 m thickness) was used for near-surface (0–0.2 m) measurements to mitigate fast neutron escape. All scales used the same instrument.

Additionally, eight representative sampling points were selected based on mean neutron counts to construct the regional SWC calibration curve. At each of these points, a 1.0 m soil profile was excavated 0.5 m from the access tube. Undisturbed soil samples were collected at 0.1 m intervals using a cutting ring (0.05 m diameter × 0.05 m height) to determine bulk density and gravimetric SWC, which were converted to volumetric SWC for calibration (Table 1).

3.1.2 Plateau-wide transect

An approximately 860-km-long, plateau-wide transect was established along broadly north-south orientation to investigate dynamic changes in deep SWC (0–5.0 m) across the LPC. A

https://doi.org/10.5194/essd-2026-437
Preprint. Discussion started: 11 August 2026

total of 86 sampling points were selected at approximately 10 km intervals, encompassing 10 farmlands, 49 forestlands, 5 shrublands, and 22 grasslands (Fig. 1). Sampling points were chosen based on two principles: (1) sufficient distance from roads and villages to minimize anthropogenic influence and (2) sufficient distance from gullies and benchlands with shallow groundwater tables to minimize groundwater effects.

At each point, a 5.2 m deep aluminum neutron probe access tube was installed, and volumetric SWC (0–5.0 m) was measured at 0.2 m intervals using a CNC 503DR Hydro probe. A total of 18 field campaigns (11 in the rainy season, June–September; seven in the dry season, October–May) were conducted between June 2013 and November 2016, generating 38,700 measurements (Fig. 2). Each campaign took three to four days to traverse the transect, and the date recorded for a campaign is its first day. The SWC calibration curve was constructed using the same method as the regional-survey scale (Table 1).

3.1.3 Local-landscape transect

The local-landscape transect is located in the Liudaogou watershed (6.9 km^2) in the wind-water cross-erosion region of the northern LPC. An approximately 1.34-km-long, east-west oriented transect was established, consisting of 135 sampling points spaced at 10 m intervals, with a few exceptions due to gullies (126 on hillslopes, nine in gullies; Fig. 1). Dominant vegetation along the transect included purple alfalfa (*Medicago sativa*), Korshinsk peashrub (*Caragana korshinskii*), and Bunge needlegrass (*Stipa bungeana*).

SWC was measured at depths of 0–3.0 m, with 0.1 m intervals at top 0.2 m and 0.2 m intervals from 0.2 to 3.0 m. Undisturbed soil samples were collected from 12 sampling points at 0.1 m intervals (0–1.0 m depth) in April, June, and October 2013 for neutron probe calibration (Table 1). A total of 18 investigations were conducted between December 2012 and October 2013, resulting in 38,880 measurements (Fig. 2).

3.1.4 Hillslope scale

Two representative hillslopes (HA and HB) were selected in the Liudaogou watershed to

https://doi.org/10.5194/essd-2026-437
Preprint. Discussion started: 11 August 2026

investigate SWC distribution at the hillslope scale. The slope gradients of HA and HB are 14° and 19°, and both slopes face west to northwest, respectively, with a deep gully serving as a natural boundary for comparative analysis. On HA and HB, 31 and 28 sampling points were selected at 10 m intervals, measured with a tape along the ground surface, respectively, to measure SWC at depths of 0–3.0 m (0.1 m intervals at top 1.0 m and 0.2 m intervals from 1.0 to 3.0 m; Fig. 1). From April 2013, the depth scheme on HB changed to 0.1 m intervals at top 0.2 m and 0.2 m intervals from 0.2 to 3.0 m.

Hillslope HA was covered with a mix of artificial and natural vegetation, including herbaceous plants (alfalfa, bunge needlegrass, *Artemisia scoparia*), trees (apricot trees), and millet. Hillslope HB consisted of abandoned fields dominated by herbaceous plants (alfalfa, bunge needlegrass). SWC measurements on HA were conducted 23 times between July 2008 and August 2011 (14,260 measurements), while HB was monitored 112 times between August 2004 and October 2016 (57,568 measurements; Fig. 2). Simultaneous measurements were conducted on both hillslopes in selected months (2010–2011). Undisturbed soil samples (0–1.0 m, 0.1 m intervals) were collected 0.5 m away from each sampling point for calibration (Table 1).

3.1.5 Plot scale

To investigate the effects of vegetation type and recovery duration on SWC distribution and dynamics, four long-term experimental plots were established in 2003 on a representative 12° northwest-facing slope in the Liudaogou watershed (Fig. 1E). Each plot (61 m × 5 m) was separated by a 0.8 m buffer zone, with a 0.1 m thick concrete wall extending 0.2 m above and 0.3 m below the soil surface to prevent inter-plot water flow.

The four plots represent typical local rainfed land use types: (1) exotic shrubland (*Caragana korshinskii*, planted in 0.7 m spaced rows, unharvested, no fertilization); (2) exotic grassland (*Medicago sativa*, planted in 0.5 m spaced rows, harvested in late August annually, no fertilization); (3) natural grassland (fallow for more than 12 years, dominated by *Stipa bungeana*); (4) arable cropland (two-year rotation of millet and soybean, planted in May, harvested in late August, fertilized with 120 kg ha^{-1} N and 26 kg ha^{-1} P annually).

https://doi.org/10.5194/essd-2026-437
Preprint. Discussion started: 11 August 2026

Eleven aluminum neutron probe access tubes (4.0 m deep) were installed at 5 m intervals along the central axis of each plot. SWC was measured at 0.1 m intervals (0–1.0 m) and 0.2 m intervals (1.0–4.0 m) mainly during the growing season (April–October), with occasional measurements in winter. A total of 124 investigations were conducted between July 2004 and May 2019, generating 12,400 measurements (Fig. 2). The dataset includes plot-averaged SWC values from 11 tubes per plot. Undisturbed soil samples (0–1.0 m, 0.1 m intervals) were collected 0.5 m away from each tube to establish the calibration curve (Table 1).

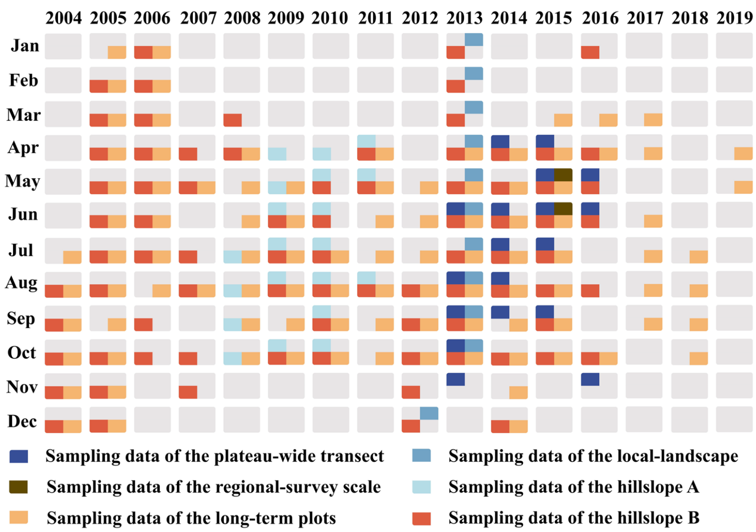

Figure 2 Sampling timeline of SWC measurements across different spatial scales.

Table 1 Calibration curves for converting neutron counts into volumetric SWC for different spatial scales.

Spatial scale	Calibration equation	R^2	*P*	References
Regional-survey scale	θ=0.5891CR+0.0089	0.93	< 0.001	Zhao et al., 2021
Plateau-wide transect scale	θ=0.5891CR+0.0089	0.93	< 0.001	Jia et al., 2015, 2017b; Zhao et al., 2017a, 2019a, 2020
Local-landscape scale	θ=0.6565CR-0.0068	0.90	< 0.001	Li et al., 2015a, 2015b, 2016, 2022
Hillslope scale	θ=0.6483CR-0.0102	0.90	< 0.001	Hu et al., 2010a; Gao and Shao, 2012; Jia et al., 2013
Plot scale	θ=0.6628CR-0.0115	0.93	< 0.001	Liu and Shao, 2016

Note: θ = volumetric soil water content ($cm^3\ cm^{-3}$); CR = neutron count ratio, the count measured in the soil divided by the standard count (685); R^2 = coefficient of determination.

https://doi.org/10.5194/essd-2026-437
Preprint. Discussion started: 11 August 2026

3.2 Soil properties

3.2.1 Physical properties

In the regional-survey scale investigation, a 0.4 m soil profile was excavated at each sampling point, and undisturbed soil samples were collected at depths of 0–0.1, 0.1–0.2, and 0.2–0.4 m using a cutting ring (0.05 m diameter × 0.05 m height). Saturated hydraulic conductivity was determined using the constant head method (Klute, 1965; Li et al., 2026). Soil water retention curves were measured via the centrifuge method (HITACHI CR21G centrifuge; 20 °C), with field capacity and wilting coefficient derived at suctions of –0.03 MPa and –1.5 MPa, respectively. Saturated SWC was determined gravimetrically after saturation and before soil water retention curve measurement. Bulk density was calculated as the ratio of dry soil mass (oven-dried at 105 °C to constant weight) to sample volume. The same methods were used at the other scales.

The dataset also includes: (1) saturated SWC, field capacity, saturated hydraulic conductivity, and bulk density at 0–0.1, 0.1–0.2, and 0.2–0.4 m for each sampling point along the plateau-wide transect; (2) saturated hydraulic conductivity and bulk density at 0–0.2 m for each sampling point along the local-landscape transect and on hillslope HB, and at 0–0.1 m on hillslope HA. All these soil physical property data were derived from single measurements, and their temporal variabilities were ignored.

3.2.2 Chemical and textural properties

Disturbed soil samples were collected along the plateau-wide transect at 0.1 m intervals (0–0.2 m), 0.2 m intervals (0.2–1.0 m), 0.5 m intervals (1.0–2.0 m), and 1.0 m intervals (2.0–5.0 m) using a soil auger. Samples were air-dried and sieved to 1 mm for the determination of soil organic carbon (SOC) content and mechanical composition. SOC content was measured via the $K_2Cr_2O_7$ oxidation method (Sparks et al., 1996), and soil texture was analyzed using a laser diffraction analyzer (Mastersizer 2000, Malvern Instrument, Malvern, England), with particle-size classes following the USDA classification. The same methods were used at the other scales.

https://doi.org/10.5194/essd-2026-437
Preprint. Discussion started: 11 August 2026

Additionally, the dataset includes: (1) soil texture data at depths of 0–0.1, 0.1–0.2, 0.2–0.4, 0.4–0.6, 0.6–0.8, 0.8–1.0, 1.0–1.5, 1.5–2.0, 2.0–3.0, 3.0–4.0, and 4.0–5.0 m for each regional sampling point; (2) SOC and texture data at 0–0.2 m depth for each sampling point along the local-landscape and on hillslope HB, and at 0–0.1 and 0.1–0.2 m on hillslope HA.

At every scale the soil samples were taken once, during the site survey: HA in July 2008, HB in September 2004, the local-landscape transect in September 2013, the plateau-wide transect in June 2013, and the regional survey between June and October 2013.

3.3 Vegetation, climate, and topography data

3.3.1 Vegetation data

During the regional-survey scale investigation of June to October 2013, land use types and vegetation characteristics were recorded at each sampling point. In forested areas, three 10 × 10 m^2 quadrats were established to assess afforestation density (via planting spacing) and to measure tree height and diameter at breast height (DBH), with mean values representing each sampling point. At grassland sampling points, three 1 × 1 m^2 quadrats were established, and vegetation coverage was visually estimated by the same team to ensure consistency. The same 10 × 10 m^2 quadrat method was used to record afforestation density along the plateau-wide transect, at the start of the first campaign in June 2013.

Along the local-landscape transect and on hillslope HB, three 1 × 1 m^2 quadrats were established at each sampling point, in September 2013 and September 2004, respectively. Aboveground plant material was collected and dried at 75 ℃ for 72 h to constant weight to determine aboveground biomass. Litterfall from each quadrat on hillslope HB was also collected and dried to determine litter mass. The value reported for each sampling point is the mean of its three quadrats, and the survey was not repeated.

3.3.2 Climate and topography data

Environmental factor data for each sampling point include: (1) Regional-survey scale and plateau-wide transect: latitude, longitude, land use type, altitude, slope gradient, slope aspect,

https://doi.org/10.5194/essd-2026-437
Preprint. Discussion started: 11 August 2026

mean annual temperature (MAT), mean annual precipitation (MAP), mean annual evaporation (MAE), mean annual aridity (MAA), and normalized difference vegetation index (NDVI); (2) Local-landscape: latitude, longitude, and altitude; (3) Hillslope scale: latitude, longitude, and altitude for each sampling point, with slope gradient and slope aspect reported for the hillslope as a whole. MAT, MAP, MAE, and MAA data were interpolated to each sampling point from records of 73 meteorological stations of the China Meteorological Data Sharing Service System (http://data.cma.cn/) for the period 1953–2013, kriged to a 100 m grid. NDVI was retrieved from MODIS NDVI data (MOD13Q1). Slope gradient and aspect were measured with a geological compass and altitude with a handheld Global Positioning System (GPS) receiver at all scales during field surveys. Latitude and longitude were obtained with the same receiver along the local-landscape transect, along the plateau-wide transect and in the regional-survey. On the two hillslopes and the plot scale, the receiver reported positions at a resolution coarser than the 10 m spacing between adjacent sampling points, and latitude and longitude were therefore determined from high-resolution satellite imagery rather than measured in the field.

4 Uncertainty analysis

4.1 Effects of instrumental error on SWC data

The accuracy of SWC measurements using neutron probes is influenced by inherent instrumental errors. Variations in neutron source stability or radioactive decay rates can lead to inconsistent counting rates even for the same soil (Preiss, 1967; Bell, 1987; Ferronsky, 2015), a phenomenon known as "random counting error" that is closely linked to counting time (Gardner, 1965; Nicolls et al., 1981; Bell, 1987). Longer counting times help approximate the true average counting rate, reducing discrepancies in repeated measurements. Visvalingam and Tandy (1972) suggested a counting time range of 30–60 s based on SWC variations across regions. After multiple experiments and calibrations, a 64 s counting time was selected to optimize counting accuracy on the LPC.

https://doi.org/10.5194/essd-2026-437
Preprint. Discussion started: 11 August 2026

4.2 Effects of soil properties on SWC data

4.2.1 Hydrogen in non-water forms

The neutron method relies on a regression equation to convert neutron counts to SWC (Visvalingam and Tandy, 1972). Most soil hydrogen is bound in soil water; however, a small fraction exists as mineral-bound crystallized/hydrated water, which is not removable by standard 105 °C drying and thus not classified as SWC (Evett, 2003). Additionally, soil organic matter contains hydrogen (Karsten et al., 1975), raising concerns about its impact on measurement accuracy (Hauser, 1984). However, mineral-bound water is stable and exerts minimal influence on neutron counts (Visvalingam and Tandy, 1972), and the hydrogen content of organic matter is substantially lower than that of soil water (Gardner and Kirkham, 1952). Given the low SOC content on the LPC, the influence of non-water hydrogen on neutron scattering is negligible.

4.2.2 Soil texture and bulk density

Soil texture and bulk density are critical factors affecting neutron counting (Holmes, 1966; McHenry and Gill, 1967). High bulk density or clay content can reduce neutron scattering and increase thermal neutron concentration around the source, potentially leading to overestimation of SWC (Visvalingam and Tandy, 1972). Thus, soil-specific calibration curves are recommended for different depths and locations (McHenry, 1963; Lal, 1974).

In this study, soil bulk density at 0–0.4 m depth (regional-survey and plateau-wide transect scales) exhibited minimal variability (coefficient of variation, CV, less than 10%), consistent with Qiao et al. (2019), who reported stable bulk density (CV < 10%) across 0–2.0 m at five LPC sites. Additionally, soil texture analysis revealed homogeneous silty loam soils across sites and depth (0–5.0 m) (Fig. 3). Calibration points were uniformly distributed during large-scale sampling to mitigate bulk density-induced biases. Given these observations, the effects of soil texture and bulk density on neutron counting were considered negligible.

https://doi.org/10.5194/essd-2026-437
Preprint. Discussion started: 11 August 2026

4.3 Effects of experimental procedures and data recording errors

Standardizing test procedures and data documentation are crucial for ensuring accuracy (Lawless et al., 1963). All data were collected by the same team following standardized protocols to minimize experimental variability. Data quality control measures included: (1) manual verification of soil depth and count rate sums in record tables against computerized results; (2) establishment of SWC upper and lower limits (based on literature and experience) to screen anomalous data, followed by manual review to retain valid data.

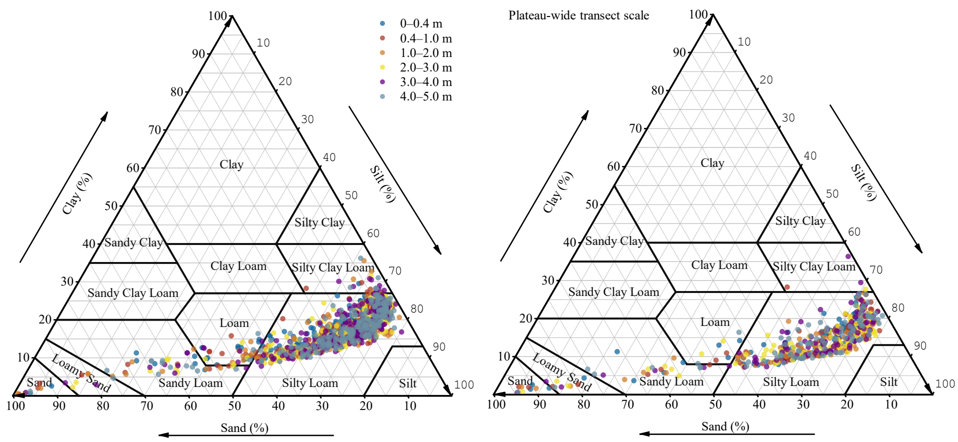

Figure 3 Soil texture at different soil depths for the regional-survey scale and plateau-wide transect.

5 Exemplary views of SWC data

A detailed analysis of the dataset is beyond the scope of this paper; however, a preliminary analysis is presented to illustrate the dataset's usability and key characteristics, laying the foundation for broader applications. This section focuses on: (1) long-term vegetation restoration effects on deep SWC at the plot scale; (2) SWC spatiotemporal variability across depths and scales; (3) spatial patterns of soil water storage (SWS) and plant-available water storage (PAWS) in the typical loess region; and (4) a preliminary comparison of the Loess-Obs network dataset with SWC products.

https://doi.org/10.5194/essd-2026-437
Preprint. Discussion started: 11 August 2026

5.1 Temporal variations in SWC under different land use types

As shown in Fig. 4, the SWC temporal dynamics across the four plots (2004–2019) can be divided into three distinct phases. Phase I (2004–2011) was characterized by rapid SWC decline at all depths: 26%–54% (0–1.0 m), 32%–63% (1.0–2.0 m), 31%–61% (2.0–3.0 m), and 29%–57% (3.0–4.0 m). This decline was attributed to higher evapotranspiration than precipitation recharge during vegetation restoration (Jia et al., 2017a), with more pronounced reductions in artificial shrublands and grasslands than in cropland and fallow land.

During Phase II (2012–2015), SWC stabilized across all plots, with CV values indicating weak (CV < 10%) or moderate (10% < CV < 100%) variability. This stability suggests that SWC reached a relatively constant level inaccessible to plant uptake (Bai et al., 2020; Jia et al., 2017a). Phase III (2016–2019) featured a rapid SWC recovery: 10%–37% (0–1.0 m), 11%–53% (1.0–2.0 m), 5%–71% (2.0–3.0 m), and 8%–49% (3.0–4.0 m), driven by recent climatic humidification on the LPC (Wang et al., 2024). Recovery was more substantial in artificial shrublands and grasslands.

During the initial planting stage (2004–2006), SWC was relatively stable across all plots. Over time, however, SWC in artificial shrublands and grasslands became significantly lower than in cropland and fallow land ($P < 0.05$), with greater differences at deeper depths. Crops and natural plants have shallow roots (0–1.0 m), leading to lower shallow SWC (Liu and Shao, 2016), while *Caragana korshinskii* and *Medicago sativa* had deep, dense roots (> 5.0 m) that depleted deep SWC (Yang et al., 2012). These differences highlight the need to consider root depth and water-use patterns when formulating vegetation restoration strategies.

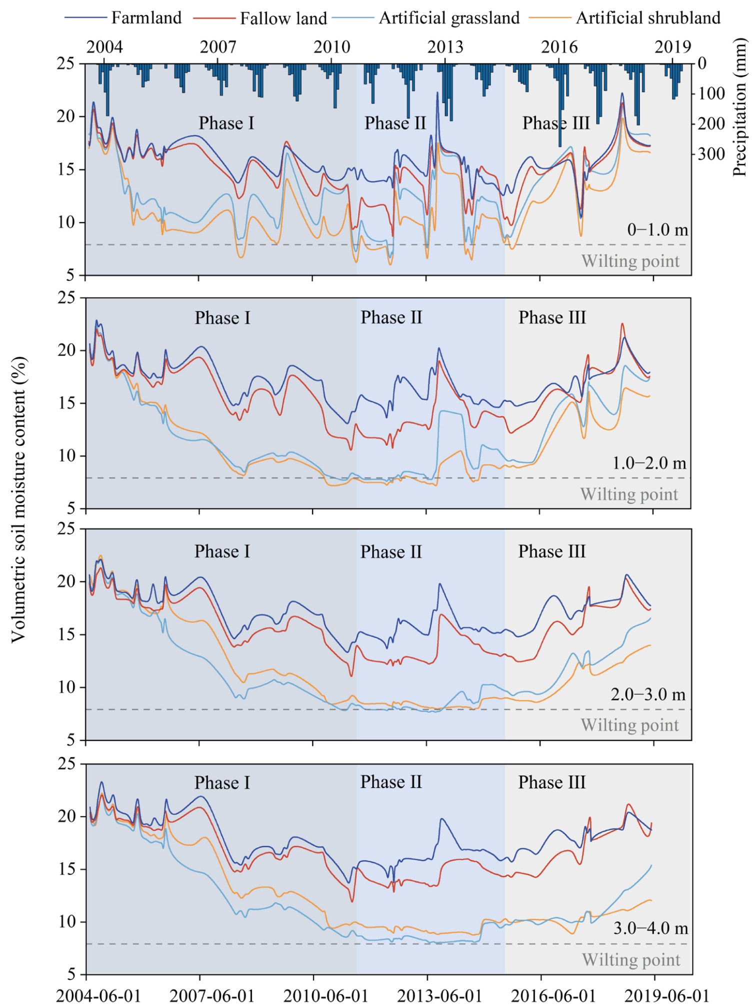

Figure 4 Temporal variations in SWC within 0–4.0 m soil profiles under different vegetation types at the plot scale.

5.2 Spatiotemporal variations in SWC across scales

5.2.1 Spatiotemporal variations in SWC at different depths

Table 2 presents the statistical characteristics of SWC spatiotemporal variability across scales and depths. Temporal variability (standard deviation of the time series, SD_T; coefficient of

https://doi.org/10.5194/essd-2026-437
Preprint. Discussion started: 11 August 2026

variation of the time series, CV_T) of shallow SWC (0–1.0 m) was higher than that of deep SWC (> 1.0 m) across all scales: For example, along the plateau-wide transect, CV_T of 0–1.0 m SWC was 14.4%, compared to 2.4% for 3.0–4.0 m SWC. This pattern, attributed to the greater susceptibility of shallow soils to evapotranspiration, root uptake, and climate change (Jia et al., 2013), which was consistent with Penna et al. (2013). Analysis of hillslopes HA and HB (Fig. 5) confirmed enhanced temporal stability of deep SWC across slope positions and seasons.

Spatial variability (standard deviation of spatial distribution, SD_S; coefficient of variation of spatial distribution, CV_S) of deep SWC (> 3.0 m) was higher than that of shallow SWC (< 2.0 m) across all scales. Along the plateau-wide transect, CV_S of 4.0–5.0 m SWC was 50.5%, compared to 40.0% for 0–1.0 m SWC. Geostatistical analysis, which addresses whether that variation is spatially structured, revealed a non-linear increase in spatial dependence with depth (Fig. 6, see *Supplement* for calculation methods): along the plateau-wide transect, the nugget ratio at 3.0–5.0 m was significantly higher than at 0–2.0 m ($P < 0.05$); along the local-landscape transect, the ratio at 2.0–3.0 m exceeded those at 0–1.0 m and 1.0–2.0 m ($P < 0.05$). Spatial dependence therefore weakens with depth, with a larger share of the variance in deep SWC occurring at distances shorter than the sampling interval and remaining unresolved by the survey. This decreased deep spatial dependence was likely driven by heterogeneous deep root distribution (Li et al., 2015c), as confirmed by hillslope spatial patterns (Fig. 5).

In conclusion, SWC spatiotemporal variability was strongly depth-dependent: shallow SWC exhibited high temporal but low spatial variability, while deep SWC showed low temporal but high spatial variability, consistently across all scales. A similar pattern has been reported at the small-watershed scale in the same region, intermediate between the hillslope and local-landscape scales (Hu et al., 2010b).

Table 2 Temporal and spatial variation characteristics of SWC at various soil depths across scales.

Spatial variables	Temporal statistics (%)	Plateau-wide transect					Local-landscape transect			Hillslope A (HA)			Hillslope B (HB)		
		0–1.0 m	1.0–2.0 m	2.0–3.0 m	3.0–4.0 m	4.0–5.0 m	0–1.0 m	1.0–2.0 m	2.0–3.0 m	0–1.0 m	1.0–2.0 m	2.0–3.0 m	0–1.0 m	1.0–2.0 m	2.0–3.0 m
Mean SWC	Mean	13.9ab	13.9ab	13.9ab	14.7ab	15.2a	14.0ab	14.1ab	14.4ab	13.9ab	14.1ab	13.9ab	13.1b	11.4c	10.4c
	Max	18.5	16.3	14.8	15.4	16.3	18.0	17.2	16.0	19.9	18.3	17.4	23.9	20.	16.1
	Min	11.2	12.0	13.0	13.9	14.5	9.7	12.9	13.7	9.2	10.5	10.5	7.1	6.8	6.6
	SD_T	2.0	1.1	0.6	0.4	0.4	2.3	1.4	0.7	2.7	2.1	1.9	3.7	2.6	1.8
	CV_T	14.5	8.0	4.2	2.4	2.5	16.2	10.2	4.6	19.4	14.9	13.9	28.0	22.8	17.0
SD_S of SWC	Mean	5.4de	5.8cd	6.2cd	7.3ab	7.7a	5.5de	6.0cd	6.5bc	3.3hi	4.7ef	4.4fg	2.8i	3.4h	4.0g
	Max	7.2	6.7	6.7	7.8	8.2	6.6	7.0	7.5	4.3	6.3	5.5	5.0	5.8	6.1
	Min	4.4	5.2	5.8	6.9	7.4	4.2	5.5	6.2	2.2	3.6	3.3	1.4	2.1	2.8
	SD_T	0.8	0.5	0.3	0.3	0.2	0.7	0.5	0.4	0.6	0.6	0.6	1.0	1.2	1.0
	CV_T	14.9	7.7	4.6	3.9	3.0	12.1	7.8	6.5	17.8	12.7	12.8	35.3	33.7	24.1
CV_S of SWC	Mean	40.1bc	42.2bc	44.9ab	49.5a	50.5a	39.5bc	42.6bc	45.2ab	24.2e	33.7d	31.7d	21.1e	29.7d	38.6c
	Max	52.9	48.4	49.7	52.2	52.9	44.8	44.6	47.4	29.0	36.6	34.9	37.7	47.1	52.6
	Min	26.3	34.0	40.0	46.9	48.4	32.0	40.1	44.1	19.0	30.8	29.8	11.4	20.4	27.1
	SD_T	8.0	4.7	3.1	1.6	1.2	3.3	1.3	1.0	3.1	1.6	1.4	5.3	6.5	7.1
	CV_T	20.1	11.3	6.9	3.3	2.3	8.2	3.1	2.1	13.0	4.7	4.6	25.0	21.8	18.4

Note: SWC = soil water content; SD_S = standard deviation of spatial distribution; CV_S = coefficient of variation of spatial distribution; SD_T = standard deviation of time series; CV_T = coefficient of variation of time series; Means followed by the same lowercase letters are not significantly different at $P < 0.05$.

https://doi.org/10.5194/essd-2026-437
Preprint. Discussion started: 11 August 2026

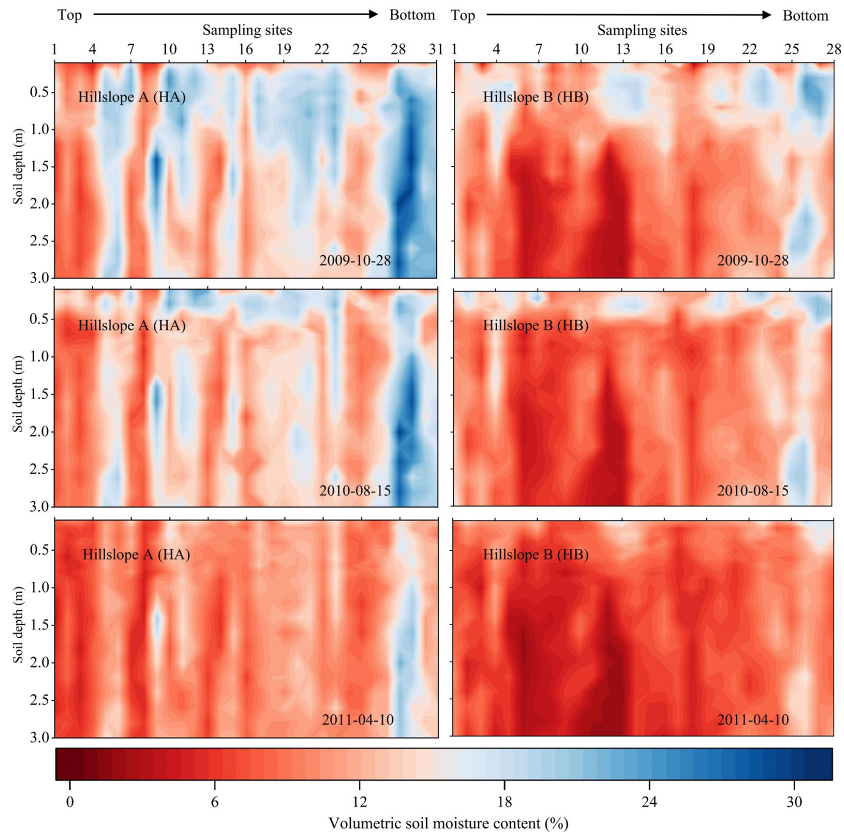

Figure 5 Spatial distribution characteristics of SWC on hillslopes HA and HB on three representative dates.

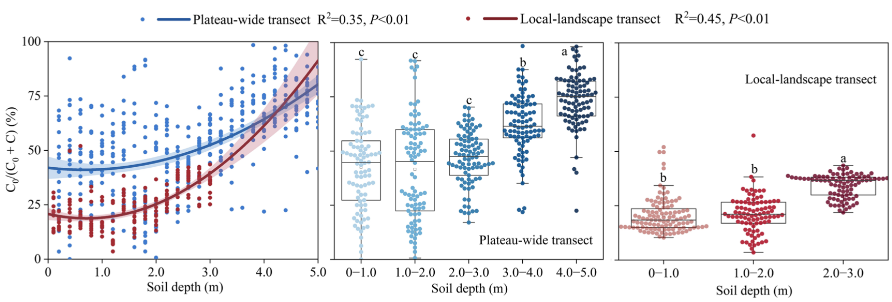

Figure 6 Spatial dependence of SWC along the plateau-wide and Local-landscape transects, shown as the nugget ratio of one semivariogram per depth layer and sampling occasion, fitted over the horizontal distance between sampling points. (A) Against soil depth. (B, C) Grouped into 1.0 m depth intervals. Note: C_0 = nugget variance; C = structural variance; $C_0/(C_0 + C)$ = nugget ratio (%); Values with the same lowercase letter indicate no significant difference at P < 0.05.

https://doi.org/10.5194/essd-2026-437
Preprint. Discussion started: 11 August 2026

5.2.2 Temporal stability of SWC at various scales

Table 3 presents the mean relative difference (MRD), its standard deviation (SDRD), and mean absolute bias error (MABE) for each sampling point at different depths (see *Supplement* for calculation methods). Along the plateau-wide transect, the MRD ranges were 153.1% (0–1.0 m), 186.0% (1.0–2.0 m), 201.1% (2.0–3.0 m), 187.5% (3.0–4.0 m), and 188.6% (4.0–5.0 m). Along the local-landscape transect, the MRD ranges were 176.0% (0–1.0 m), 200.8% (1–2.0 m), and 235.7% (2.0–3.0 m). The magnitudes of MRD were lower in shallow soils (0–1.0 m) than in deep soils (> 1.0 m), reflecting the reduced spatial variability in shallow layers (Table 2). Both the mean SDRD and the mean MABE decreased with increasing soil depth, indicating enhanced temporal stability of deep SWC.

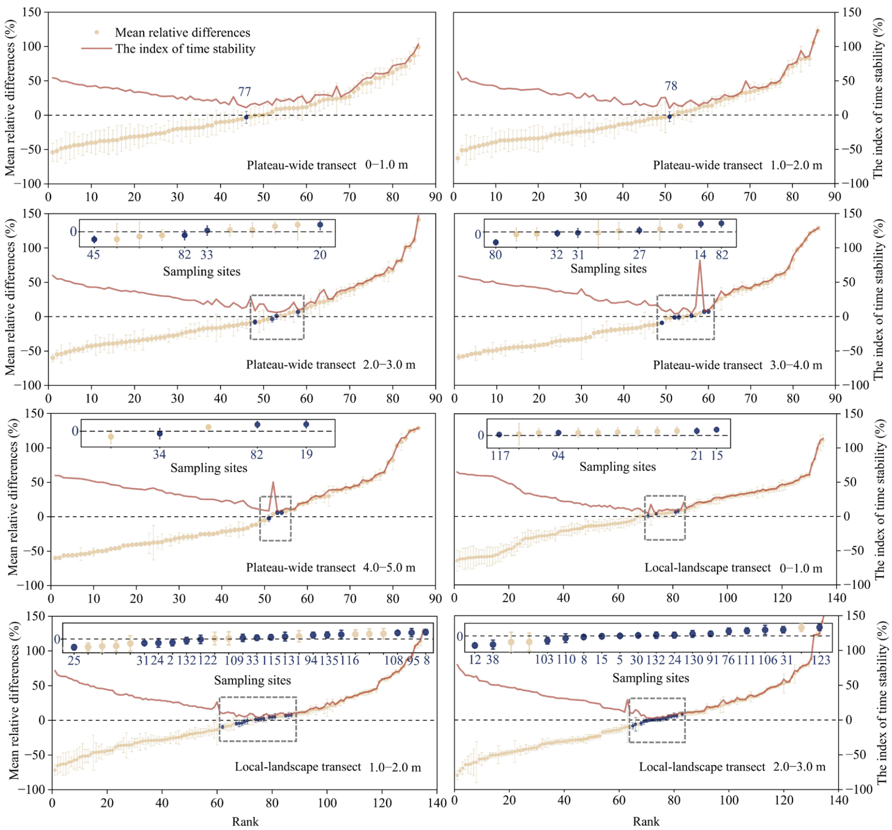

Figure 7 Temporal stability of SWC along the plateau-wide and local-landscape transects. Note:

https://doi.org/10.5194/essd-2026-437
Preprint. Discussion started: 11 August 2026

Yellow symbols are the ranked mean relative differences (MRD), with error bars showing mean absolute bias error (MABE), and the red line is the index of temporal stability (ITS). Blue symbols are the time-stable points (MABE < 5%, ITS < 10%), numbered in the insets. The MABE threshold was relaxed to 10% for the 0–1.0 m and 1.0–2.0 m layers of the plateau-wide transect.

Time-stable points (identified by an index of temporal stability, ITS < 10%, and MABE < 5%) were selected to estimate the mean SWC at each depth (Fig. 7). Along the plateau-wide transect, no time-stable points were identified at 0–1.0 m or 1.0–2.0 m. However, four, six, and three points met the criteria at 2.0–3.0 m, 3.0–4.0 m, and 4.0–5.0 m, respectively. For the local-landscape transect, four, 16, and 17 time-stable points were found at 0–1.0 m, 1.0–2.0 m, and 2.0–3.0 m, respectively. Notably, the 82nd sampling point along the plateau-wide transect effectively represented the mean SWC for the 2.0–3.0 m, 3.0–4.0 m, and 4.0–5.0 m layers. Conversely, no single point was found to be representative across all measured depths.

Table 3 Statistical metrics of SWC temporal stability at different depths along the Plateau-wide and local-landscape transects.

Parameters		Plateau-wide transect					Local-landscape transect		
		0–1.0 m	1.0–2.0 m	2.0–3.0 m	3.0–4.0 m	4.0–5.0 m	0–1.0 m	1.0–2.0 m	2.0–3.0 m
MRD (%)	Min	-54.0	-62.9	-59.9	-58.8	-59.8	-64.6	-71.6	-79.6
	Max	99.1	123.1	141.1	128.8	128.8	111.4	129.3	156.2
	Range	153.1	186.0	201.1	187.5	188.7	176.0	200.9	235.7
	N_1	7	8	6	8	1	13	15	11
SDRD (%)	Mean	17.4	14.1	10.2	7.8	7.0	7.7	6.8	5.4
	Min	7.6	3.0	2.0	1.3	1.1	2.7	2.6	1.4
	Max	36.0	46.7	40.6	29.4	34.9	27.6	23.1	27.2
	Range	28.4	43.7	38.7	28.1	33.9	24.9	20.5	25.
	N_2	0	4	21	35	43	20	46	90
MABE (%)	Mean	14.1	11.3	8.0	6.0	4.8	7.0	6.2	4.7
	Min	6.2	5.3	2.3	1.9	1.	1.7	1.6	0.7
	Max	23.2	22.5	23.2	29.9	25.2	16.8	25.3	29.1
	Range	17.0	17.2	21.0	28.0	23.7	15.1	23.7	28.4
	N_3	0	0	24	48	61	44	73	106

Note: MRD = mean relative difference; SDRD = standard deviation of relative difference; MABE = mean absolute bias error; N_1, N_2, and N_3 represent the number of sampling points with MRD

https://doi.org/10.5194/essd-2026-437
Preprint. Discussion started: 11 August 2026

ranging from -5 to 5%, SDRD < 10%, and MABE < 5%, respectively.

For the shallow layers (0–1.0 m and 1.0–2.0 m) along the plateau-wide transect, the MABE threshold was relaxed to 10% following established protocols (Martínez-Fernández and Ceballos, 2005; Wang et al., 2015). Under this adjusted criterion, the 77th sampling point (MABE < 10%, ITS = 11%) and the 78th point (MABE < 10%, ITS = 10%) were recommended as the optimal time-stable representatives for the 0–1.0 m and 1.0–2.0 m layers, respectively (Fig. 7).

5.3 Spatial patterns of soil water storage at the regional-survey scale

Soil water storage (SWS) and plant-available water storage (PAWS) in the 0–5 m profile were calculated to characterize the regional hydrological status of the LPC (Table 4, see *Supplement* for calculation methods). PAWS was defined as the difference between the measured volumetric SWC and the wilting point, integrated over the 0–0.4 m depth.

At the regional-survey scale, both SWS and PAWS exhibited a distinct zonal distribution, decreasing significantly from the southeast to the northwest (Fig. 8). This spatial pattern was strongly correlated with the regional precipitation gradient (R^2 = 0.87, P < 0.001), which is the primary driver of soil water recharge in this arid and semi-arid region. Specifically, the mean SWS in the southeastern semi-humid zone (MAP > 600 mm) exceeded 800 mm, while in the northwestern arid zone (MAP < 300 mm), SWS was consistently below 450 mm.

Land use type further modulated this climatic pattern. Across the entire region, farmlands had the highest mean PAWS (29 ± 19 mm), followed by forestlands (24 ± 18 mm), shrublands (19 ± 15 mm) and natural grasslands (14 ± 15 mm). In the water-limited northwest, forestlands exhibited the lowest PAWS values (< 10 mm), indicating potential hydrological stress for deep-rooted woody vegetation. These spatial patterns establish a critical baseline for quantifying the regional water budget and assessing the ecological carrying capacity of the LPC under ongoing vegetation restoration efforts.

https://doi.org/10.5194/essd-2026-437
Preprint. Discussion started: 11 August 2026

Table 4 Descriptive statistics of SWS and PAWS in the typical loess region of the LPC.

Water storage	Soil layer (m)	Max (mm)	Min (mm)	Mean (mm)	SD (mm)	CV (%)
SWS	0–1.0	358.1	45.8	156.1	54.6	35.0
	1.0–5.0	1264.7	202.3	586.8	256.0	43.6
	0–5.0	1581.3	250.7	742.9	299.0	40.2
PAWS	0–0.4	100.3	0.0	21.1	17.8	84.5

Note: SWS = soil water storage; PAWS = plant-available water storage; Max = maximum; Min = minimum; SD = standard deviation; CV = coefficient of variation; n=243.

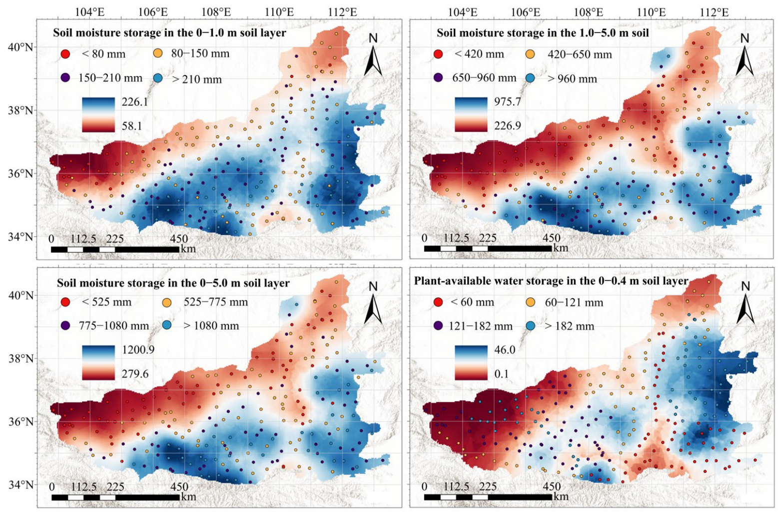

Figure 8 Spatial variability of soil water storage at various depths and plant-available water storage in the surface soil in the typical loess region of the LPC.

5.4 Preliminary comparison with the SWC products

To illustrate the dataset's utility for benchmarking land surface models (LSMs), the SWC measurements of plateau-wide transect were compared against six widely used products (GLDAS-Noah, GLDAS-CLSM, MERRA-2, NCEP-CFSR/v2, ERA5-Land, and JRA-3Q) over 2013–2016 (Fig. 9). The products consistently overestimated the observed SWC, with the overestimation growing larger with depth: values were close to the observations near the surface but diverged significantly in the deeper layers, indicating substantial and growing uncertainty at depth. JRA-3Q stood out,

https://doi.org/10.5194/essd-2026-437
Preprint. Discussion started: 11 August 2026

overestimating SWC throughout the profile and producing an unrealistically strong seasonal cycle. Among the products, GLDAS-Noah most closely matched the observations, yet all of them poorly represented the deeper layers (Fig. 9). This decline in accuracy with depth reflects the scarcity of deep *in situ* measurements available for model calibration.

These results also highlight a broader observational gap. Satellite-based retrievals such as SMOS are confined to the top few centimeters, and LSM-driven products rarely extend below 3.0 m. This limitation is particularly consequential for the LPC, where deep-rooted exotic species such as *Caragana korshinskii* and *Medicago sativa* develop root systems that extend to or even beyond 5.0 m, making deep-layer SWC a critical yet poorly constrained component of the regional water balance. The Loess-Obs dataset, with continuous *in situ* measurements spanning the full 0–5.0 m profile over 16 years, therefore offers a unique benchmark for improving deep SWC simulations and informing next-generation data product development in arid and semi-arid regions.

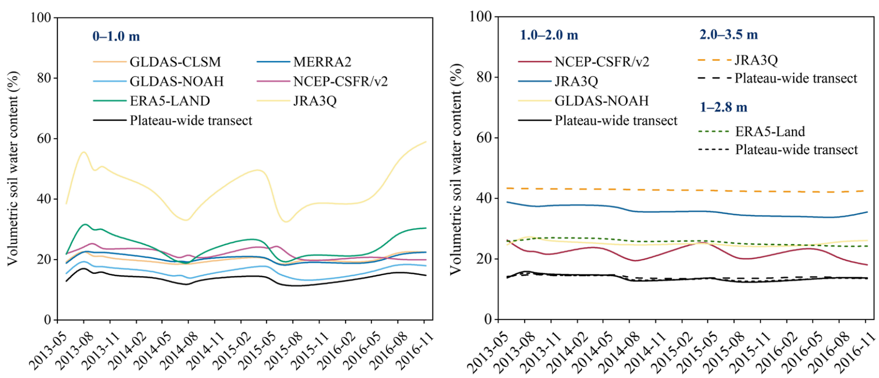

Figure 9 Comparison of observed SWC along the plateau-wide transect with SWC products.

5.5 Implications for hydrological modeling and ecosystem management

5.5.1 Validating satellite-derived SWC products and land surface models

The Loess-Obs network dataset addresses a critical validation gap for both satellite

https://doi.org/10.5194/essd-2026-437
Preprint. Discussion started: 11 August 2026

remote sensing products and LSMs, particularly in deep soil layers. Most current satellite missions (e.g., SMOS, SMAP, Sentinel-1) primarily retrieve SWC in the top 0–0.05 m to 0–0.1 m, while LSMs often simplify the vertical representation of soil hydrology or lack robust parameterization for deep root water uptake.

The multi-scale, deep-profile measurements provide a unique opportunity to: (1) evaluate the performance of downscaled satellite SWC products in heterogeneous loess landscapes; (2) calibrate the soil hydraulic parameters and root water uptake functions in LSMs for deep soil layers (> 1.0 m); and (3) quantify the model uncertainty introduced by ignoring depth-dependent spatiotemporal variability (Section 5.2.1). Preliminary validation using ERA5 and GLDAS-Noah data shows significant discrepancies in the 0.28–1.0 m layer (root mean square error, RMSE > 6 %; Yan et al., 2026), highlighting the need for model improvement using *in situ* data from this dataset.

5.5.2 Developing upscaling methodologies for SWC

The identification of time-stable sampling points (Section 5.2.2) offers a cost-effective framework for upscaling point-scale SWC measurements to hillslope or regional-survey scales. Traditional SWC monitoring at large scales is often constrained by labor and resource costs. The Loess-Obs network dataset demonstrates that a small number of strategically selected time-stable points can accurately estimate the mean SWC of deep soil layers (≥ 2.0 m) with MABE < 5%.

This finding has two key implications: (1) it enables the design of optimized monitoring networks that reduce sampling intensity without sacrificing accuracy; and (2) it provides a robust reference for validating geostatistical and machine learning-based upscaling methods. By integrating the temporal stability index with environmental covariates (e.g., topography, vegetation), researchers can develop transferable upscaling models applicable to other arid and semi-arid regions with similar loessial soils.

https://doi.org/10.5194/essd-2026-437
Preprint. Discussion started: 11 August 2026

5.5.3 Informing sustainable vegetation restoration and land management

The 15-year time series (Section 5.1) provide empirical evidence for the long-term hydrological impacts of different vegetation restoration strategies, which is critical for guiding sustainable land management on the LPC. The data clearly show that the introduction of exotic deep-rooted species (e.g., *Caragana korshinskii*, *Medicago sativa*) can lead to significant depletion of deep soil water, potentially forming a dry soil layer that is difficult to recover in the short term.

However, the observed SWC recovery phase (2016–2019) also indicates that the hydrological system may be resilient to climatic variability. These insights support the development of adaptive management strategies: (1) prioritizing native shallow-rooted grasses in water-limited areas to maintain the soil water balance; (2) implementing mixed vegetation systems to avoid excessive deep-water consumption; and (3) using the regional SWS and PAWS maps (Section 5.3) to delineate zones where afforestation is ecologically feasible. Ultimately, the Loess-Obs network dataset serves as a scientific basis for reconciling ecological restoration goals with hydrological sustainability on the LPC.

6 Data availability

The dataset, titled "A dataset of soil water measurements at multiple scales and depths on China's Loess Plateau" is archived at Zenodo and is openly available at https://zenodo.org/records/21859310 (Zhao et al., 2026) under a Creative Commons Attribution 4.0 International licence. It is organised as six archives, one for each observation scale described in Sect. 3.1, with the two hillslopes held separately: regional-survey.zip (Sect. 3.1.1), plateau_wide_transect.zip (Sect. 3.1.2), local_andscape_transect.zip (Sect. 3.1.3), hillslope_A.zip and hillslope_B.zip (Sect. 3.1.4), and plot.zip (Sect. 3.1.5). Each archive contains the measurements as comma-separated values, a metadata file in JSON giving the coverage, site setting, calibration equation and measurement protocol of that scale, and a data dictionary defining every column of every file in the archive. A README at the top level describes the structure

https://doi.org/10.5194/essd-2026-437
Preprint. Discussion started: 11 August 2026

of the data set and the conventions common to all six archives.

7 Conclusions

This study presents a comprehensive, long-term (2004–2019) SWC dataset derived from the Loess-Obs network, covering five spatial scales (plot, hillslope, local-landscape, plateau-wide transect, and regional-survey scale) and deep soil profiles (3.0–5.0 m) on the LPC. Rigorous calibration of neutron probes, standardized field sampling protocols, and stringent quality control measures ensure the high accuracy, reliability, and comparability of the volumetric SWC data, which are further complemented by a suite of environmental covariates (soil properties, topography, vegetation, and meteorology) to support multi-disciplinary research applications.

Key findings from preliminary data analysis include: (1) exotic deep-rooted vegetation (*Caragana korshinskii*, *Medicago sativa*) accelerates deep SWC depletion compared to cropland and naturally restored fallow land, with SWC temporal dynamics exhibiting three phases (decline, stabilization, recovery) driven by vegetation growth and recent climatic humidification; (2) spatiotemporal variability of SWC is depth-dependent, with temporal variability decreasing with depth and spatial variability increasing with depth, across all monitoring scales; (3) time-stable sampling points can be used effectively to characterize mean SWC of deep layers (≥ 2.0 m), providing a cost-effective upscaling tool; (4) regional soil water storage decreases from southeast to northwest, establishing a baseline for LPC water budget assessments; and (5) the performance of land surface models in simulating SWC deteriorates with soil depth, highlighting the importance of deep *in situ* observations for model calibration.

This dataset addresses a critical gap in existing SWC observations by integrating long-term, multi-scale, and deep-profile measurements across a geomorphologically complex loessial landscape, in contrast to the shallow retrievals of satellite products (e.g., SMOS) and the limited depth coverage of short-term *in situ* networks (e.g., SoilSCAPE). It serves as a pivotal benchmark for validating satellite- and model-derived SWC products, calibrating hydrological and land surface models (including the

https://doi.org/10.5194/essd-2026-437
Preprint. Discussion started: 11 August 2026

improvement of soil hydrological parameterization in Earth system models, e.g., CMIP6) and developing robust upscaling methodologies that bridge point-scale observations to landscape and regional-survey scales. Beyond technical applications, this dataset advances understanding of soil hydrology-vegetation-climate feedbacks, supporting evidence-based decision-making for sustainable land management, ecological restoration, and water resource optimization in the Yellow River Basin and similar arid and semi-arid regions worldwide.

Author contributions

WZ and XJ conceptualized the study. WZ, XJ, WH, XL, CZ, LG, YJ and MS performed the analysis and created illustrations. WZ and XJ wrote the manuscript with input from all authors. WZ, XJ, WH, XL, CZ, LG, YJ and MS reviewed and revised the paper.

Competing interests

The authors declare that they have no conflict of interest.

Acknowledgements

We are grateful to all those who contributed to the data monitoring, quality control, and processing, whose collective efforts made this dataset possible.

Financial support

This work was supported by the National Natural Science Foundation of China (U2444217).

References

Babaeian, E., Sadeghi, M., Jones, S. B., Montzka, C., Vereecken, H., and Tuller, M.: Ground, proximal, and satellite remote sensing of soil moisture, Rev. Geophys, 57(2), 530–616, 2019.

Bai, X., Jia, X., Jia, Y., and Hu, W.: Modeling long-term soil water dynamics in response to land-use change in a semi-arid area, J. Hydrol, 585, 124824, 2020.

Beck, H. E., Pan, M., Miralles, D. G., Reichle, R. H., Dorigo, W. A., Hahn, S., Sheffield, J., Karthikeyan, L., Balsamo, G., Parinussa, R. M., van Dijk, A. I. J. M., Du, J. Y., Kimball, J. S., Vergopolan, N., and Wood, E. F.: Evaluation of 18 satellite-and model-based soil moisture products using in situ measurements from 826 sensors. Hydrol. Earth Syst. Sci., 25(1), 17–40, 2021.

Bell, J. P.: Neutron probe practice. 3rd ed. Hydrology Report 19. Available at (verified 22 Jan. 2008). Institute of Hydrology, Wallingford, Oxon, UK. 1987.

Biswas, A., Cresswell, H. P., Chau, H. W., Rossel, R. A. V., and Si, B. C.: Separating scale-specific soil spatial variability: A comparison of multi-resolution analysis and empirical mode decomposition, Geoderma, 209, 57–64, 2013.

Chen, Y. P., Wang, K. B., Fu, B. J., Wang, Y. F., Tian, H. W., Wang, Y., and Zhang, Y.: 65% cover is the sustainable vegetation threshold on the Loess Plateau, Environ. Sci. Ecotechnol., 22, 100442, 2024.

Cooper, H. M., Bennett, E., Blake, J., Blyth, E., Boorman, D., Cooper, E., Evans, J., Fry, M., Jenkins, A., Morrison, R., Rylett, D., Stanley, S., Szczykulska, M., Trill, E., Antoniou, V., Askquith-Ellis, A., Ball, L., Brooks, M., Clarke, M. A., Cowan, N., Cumming, A., Farrand, P., Hitt, O., Lord, W., Scarlett, P., Swain, O., Thornton, J., Warwick, A., and Winterbourn, B.: COSMOS-UK: national soil moisture and hydrometeorology data for environmental science research, Earth Syst. Sci. Data, 13(4), 1737–1757, 2021.

Crow, W. T., Berg, A. A., Cosh, M. H., Loew, A., Mohanty, B. P., Panciera, R., de Rosnay, P., Ryu, D., and Walker, J. P.: Upscaling sparse ground-based soil moisture observations for the validation of coarse-resolution satellite soil moisture products, Rev. Geophys., 50, 2, 2012.

Desilets, D., Zreda, M., and Ferré, T. P.: Nature's neutron probe: Land surface hydrology at an elusive scale with cosmic rays, Water Resour. Res., 46(11), 2010.

Duan, S. B., Li, Z. L., Li, H., Göttsche, F. M., Wu, H., Zhao, W., Leng, P., Zhang, X., and Coll, C.: Validation of Collection 6 MODIS land surface temperature product using in situ measurements, Remote Sens. Environ., 225, 16–29, 2019.

Entekhabi, D., Njoku, E. G., O'neill, P. E., Kellogg, K. H., Crow, W. T., Edelstein, W.

N., Entin, J. K., Goodman, S. D., Jackson, T. J., Johnson, J., Kimball, J., Piepmeier, J. R., Koster, R. D., Martin, N., McDonald, K. C., Moghaddam, M., Moran, S., Reichle, R., Shi, J. C., Spencer, M. W., Thurman, S. W., Tsang, L., and Van Zyl, J.: The soil moisture active passive (SMAP) mission, Proc. IEEE, 98(5), 704–716, 2010.

Evett, S. R.: Soil water measurement by neutron thermalization, Encyclopedia of water science, 889-893, 2003.

Ferronsky, V. I.: Nuclear geophysics: applications in hydrology, hydrogeology, engineering geology, agriculture and environmental science, Springer, 2015.

Gao, L., and Shao, M.: Temporal stability of soil water storage in diverse soil layers, Catena, 95, 24–32, 2012.

Gao, X., Wu, P., Zhao, X., Shi, Y., Wang, J., and Zhang, B.: Soil moisture variability along transects over a well-developed gully in the Loess Plateau, China, Catena, 87(3), 357–367, 2011.

Gardner, W. H.: Water content, 104–114. In: C. A. Black (ed.). Methods of soil analysis. Part 1, Monograph No. 9. Am. Soc. Agron., Madison, WI, 1965.

Gardner, W., and Kirkham, D.: Determination of soil moisture by neutron scattering, Soil Sci., 73(5), 391–402, 1952.

Hauser, V. L.: Neutron meter calibration and error control, T. ASAE, 27(3), 722–728, 1984.

Holmes, J. W.: Influence of bulk density of the soil on neutron moisture meter calibration, Soil Sci., 102, 355–360, 1966.

Hu, W., Shao, M., and Reichardt, K.: Using a new criterion to identify sites for mean soil water storage evaluation, Soil Sci. Soc. Am. J., 74(3), 762–773, 2010a.

Hu, W., Shao, M. A., Han, F. P., Reichardt, K., Tan, J.: Watershed scale temporal stability of soil water content. Geoderma, 158(3–4), 181–198, 2010b.

Huang, L. M., and Shao, M. A.: Advances and perspectives on soil water research in China's Loess Plateau, Earth Sci. Rev., 199, 102962, 2019.

Jia, X. X., Shao, M. A., Wei, X. R., and Wang, Y. Q.: Hillslope scale temporal stability

https://doi.org/10.5194/essd-2026-437
Preprint. Discussion started: 11 August 2026

of soil water storage in diverse soil layers, J. Hydrol., 498, 254–264, 2013.

Jia, X. X., Shao, M. A., Zhang, C. C., and Zhao, C. L.: Regional temporal persistence of dried soil layer along south–north transect of the Loess Plateau, China, J. Hydrol., 528, 152–160, 2015.

Jia, X. X., Shao, M. A., Zhao, C. L., and Zhang, C. C.: Spatiotemporal characteristics of soil water storage along regional transect on the Loess Plateau, China, CLEAN–Soil, Air, Water, 45, 1, 2017b.

Jia, X. X., Shao, M. A., Zhu, Y. J., and Luo, Y.: Soil moisture decline due to afforestation across the Loess Plateau, China, Journal of Hydrology, 546, 113–122, 2017a.

Jia, X. X., Zhu, P., Wei, X. R., Zhu, Y. J., Huang, M. B., Hu, W., Wang, Y. Q., Turkeltaub, T., Binley, A., Horton, R., and Shao, M. A.: Bringing ancient loess critical zones into a new era of sustainable development goals, Earth Sci. Rev., 255, 104852, 2024.

Jia, X., Zhao, C., Wang, Y., Zhu, Y., Wei, X., and Shao, M. A.: Traditional dry soil layer index method overestimates soil desiccation severity following conversion of cropland into forest and grassland on China's Loess Plateau, Agr. Ecosyst. Environ., 291, 106794, 2020.

Jian, S., Zhao, C., Fang, S., and Yu, K.: Effects of different vegetation restoration on soil water storage and water balance in the Chinese Loess Plateau, Agric. Water Manage., 206, 85–96, 2015.

Karsten, J. H. M., Deist, J., and DeWaal, H. O.: A method of predicting the calibration curve for neutron moisture meter, Agrochemophysica, 7, 49–54, 1975.

Kirkby, M. J.: Water in the critical zone: soil, water and life from profile to planet, Soil, 2(4), 631–645, 2016.

Klute, A. 1965. Laboratory measurement of hydraulic conductivity of saturated soil. In: C.A. Black, editor, Methods of soil analysis. Part 1. Physical and mineralogical properties, including statistics of measurement and sampling. Agron. Monogr. 9. ASA and SSSA, Madison, WI. p. 210–221.

Kodikara, J., Rajeev, P., Chan, D., and Gallage, C.: Soil moisture monitoring at the field

https://doi.org/10.5194/essd-2026-437
Preprint. Discussion started: 11 August 2026

scale using neutron probe, Can. Geotech. J., 51(3), 332–345, 2014.

Lal, R.: The effect of soil texture and density on the neutron and density probe calibration for some tropical soils, Soil Sci., 117, 183–190, 1974.

Lawless, G. P., MacGillivray, N. A., and Nixon, P. R.: Soil moisture interface effects upon readings of neutron moisture probes, Soil Sci. Soc. Am. J., 27(5), 502–507, 1963.

Li, B. B., Li, P. P., Zhang, W. T., Ji, J. Y., Liu, G. B., and Xu, M. X.: Deep soil moisture limits the sustainable vegetation restoration in arid and semi-arid Loess Plateau, Geoderma, 399, 115122, 2021.

Li, J. B., Hu, W., Langer, S., Malcolm, B. J., Maley, S., Jenkins, H., and Carey, P.: Catch crops promote soil physical recovery after forage crop grazing, Soil and Tillage Research, 255, 106778, 2026.

Li, X. Z., Shao, M. A., Jia, X. X. and Wei, X. R.: Landscape-scale temporal stability of soil water storage within profiles on the semiarid Loess Plateau of China, J. Soils Sediments, 15, 949–961, 2015c.

Li, X., Jia, X., and Wei, X.: Profile distribution of soil–water content and its temporal stability along a 1340-m long transect on the Loess Plateau, China, Catena, 137, 77–86, 2016.

Li, X., Shao, M. A., and Xu, X.: Prediction of soil water storage using temporal stability in different landscape positions on the northern loess plateau, China, Hydrol. Processes, 36(9), e14671, 2022.

Li, X., Shao, M. A., Jia, X., Wei, X., and He, L.: Depth persistence of the spatial pattern of soil–water storage along a small transect in the Loess Plateau of China, J. Hydrol., 529, 685–695, 2015a.

Li, X., Shao, M., Jia, X., and Wei, X.: Landscape-scale temporal stability of soil water storage within profiles on the semiarid Loess Plateau of China, J. Soils Sediments, 15, 949–961, 2015b.

Li, X. Z., Xu, X. L., Liu, W., He, L., Xu, C. H., Zhang, R. F., Chen, L., and Wang, K. L.: Revealing the scale-specific influence of meteorological controls on soil water

https://doi.org/10.5194/essd-2026-437
Preprint. Discussion started: 11 August 2026

content in a karst depression using wavelet coherency, Agr. Ecosyst. Environ., 279, 89–99, 2019.

Liu, B., and Shao, M. A.: Modeling soil–water dynamics and soil–water carrying capacity for vegetation on the Loess Plateau, China, Agric. Water Manage., 159, 176–184, 2015.

Liu, B., and Shao, M. A.: Response of soil water dynamics to precipitation years under different vegetation types on the northern Loess Plateau, China, J. Arid Land, 8, 47−59, 2016.

Martínez-Fernández, J., and Ceballos, A.: Mean soil moisture estimation using temporal stability analysis, J. Hydrol., 312(1−4), 28−38, 2005.

McHenry, F. R., and Gill, A. C.: The influence of bulk density, slow neutron absorbers, and time of the calibration of the neutron moisture probes. Isotopes and Radiation Techniques in Soil Physics and Irrigation Studies, FAO/IAEA Symposium, Istanbul, June 12–16, 83–97, 1967.

McHenry, F. R.: Theory and application of neutron scattering in the measurement of soil moisture, Soil Sci., 95, 294–307, 1963.

Mertens, J., Madsen, H., Kristensen, M., Jacques, D., and Feyen, J.: Sensitivity of soil parameters in unsaturated zone modelling and the relation between effective, laboratory and in situ estimates, Hydrol. Processes, 19(8), 1611–1633, 2005.

Nicolls, K. D., Honeysett, J. L., and Hughes, M. W.: Instrument design, 24–34. In: E. L. Greacen. Soil water assessment by the neutron method. CSIRO, 314 Albert St., East Melbourne, Australia 3002, 1981.

Peng, J., Albergel, C., Balenzano, A., Brocca, L., Cartus, O., Cosh, M. H., Crow, W. T., Dabrowska-Zielinska, K., Dadson, S., Davidson, M. W., de Rosnay, P., Dorigo, W., Gruber, A., Hagemann, S., Hirschi, M., Kerr, Y. H., Lovergine, F., Mahecha, M. D., Marzahn, P., Mattia, F., Musial, J. P., Preuschmann, S., Reichle, R. H., Satalino, G., Silgram, M., van Bodegom, P. M., Verhoest, N. E., Wagner, W., Walker, J. P., Wegmüller, U., and Loew, A.: A roadmap for high-resolution satellite soil moisture applications-confronting product characteristics with user requirements, Remote

https://doi.org/10.5194/essd-2026-437
Preprint. Discussion started: 11 August 2026

Sens. Environ., 252, 112162, 2021.

Penna, D., Brocca, L., Borga, M., and Dalla Fontana, G.: Soil moisture temporal stability at different depths on two alpine hillslopes during wet and dry periods, J. Hydrol., 477, 55−71, 2013.

Preiss, K.: Design of a Neutron Scattering Water Content Gage for Soils, Isotope Techniques in the Hydrologic Cycle, 11, 22–27, 1967.

Qiao, J., Zhu, Y., Jia, X., Huang, L., and Shao, M. A.: Development of pedotransfer functions for predicting the bulk density in the critical zone on the Loess Plateau, China, J. Soils Sediments, 19, 366–372, 2019.

Rao, P., Wang, Y., Wang, F., Liu, Y., Wang, X., and Wang, Z.: Daily soil moisture mapping at 1 km resolution based on SMAP data for desertification areas in northern China, Earth Syst. Sci. Data, 14(7), 3053–3073, 2022.

Rodell, M., Houser, P., Peters-Lidard, C., Kato, H., Kumar, S., Gottschalck, J., Mitchell, K., Meng, J.: Nasa/Noaa's global land data assimilation system (GLDAS): Recent results and future plans. In Proceedings of the ECMWF/ELDAS Workshop on Land Surface Assimilation (pp. 61-68), 2004.

Sparks, D. L., Page, A. L., Helmke, P. A., Loeppert, R. H., Soltanpour, P. N., Tabatabai, M. A., Johnston, C. T., and Sumner, M. E.: Methods of Soil Analysis. Part 3: Chemical Methods. Soil Science Society of America and American Society of Agronomy, Madison, WI, 1996.

Tavakol, A., McDonough, K. R., Rahmani, V., Hutchinson, S. L., and Hutchinson, J. S.: The soil moisture data bank: The ground-based, model-based, and satellite-based soil moisture data, RSASE., 24, 100649, 2021.

Visvalingam, M., and Tandy, J. D.: The neutron method for measuring soil moisture content-a review, Eur. J. Soil Sci., 23(4), 499–511, 1972.

Wang, F., Zhao, G. J., Sun, W. Y., Liu, Y. L.: Institute of Soil and Water Conservation, Chinese Academy of Sciences and Ministry of Water Resources. A dataset on the dynamics of soil moisture content under major land uses (highly productive agricultural land, orchards, secondary forest areas) (2018–2019), 2019,

https://doi.org/10.5194/essd-2026-437
Preprint. Discussion started: 11 August 2026

https://www.geodata.cn/main/#/face_science_detail?typeName=face_science&guid=32375063973139.

Wang, Y., Hu, W., Sun, H., Zhao, Y., Zhang, P., Li, Z., Zhou, Z., Tong, Y., Liu, S., Zhou, J., Huang, M., Jia, X., Clothier, B., Shao, M., Zhou, W., and An, Z.: Soil moisture decline in China's monsoon loess critical zone: More a result of land-use conversion than climate change, PNAS., 121(15), e2322127121, 2024.

Wang, Y., Hu, W., Zhu, Y., Shao, M. A., Xiao, S., and Zhang, C.: Vertical distribution and temporal stability of soil water in 21-m profiles under different land uses on the Loess Plateau in China. J. Hydrol., 527, 543−554, 2015.

Xu, M. X.: Institute of Soil and Water Conservation, Chinese Academy of Sciences and Ministry of Water Resources. Spatial and temporal distribution of soil moisture content in agro-ecosystems (2001–2017), 2018. https://www.geodata.cn/main/#/face_science_detail?typeName=face_science&guid=164316459314496.

Yan, S., Weng, B., Dong, Z., Yan, D., and Fu, Q.: Simulation of soil moisture and drought prediction in middle reaches of the Yellow River based on machine learning, Agric. Water Manag., 323, 110068, 2026.

Yang, L., Wei, W., Chen, L., Jia, F., and Mo, B.: Spatial variations of shallow and deep soil moisture in the semi-arid Loess Plateau, China, Hydrol. Earth Syst. Sci., 16(9), 3199–3217, 2012.

Yang, X., Liu, T., and Yuan, B.: The Loess Plateau of China: aeolian sedimentation and fluvial erosion, both with superlative rates. In Geomorphological landscapes of the world (pp. 275–282). Dordrecht: Springer Netherlands, 2009.

Yu, B., Liu, G., Liu, Q., Wang, X., Feng, J., and Huang, C.: Soil moisture variations at different topographic domains and land use types in the semi-arid Loess Plateau, China, Catena, 165, 125–132, 2018.

Zhao, C., Jia, X., and Zhang, X.: Using pedo-transfer functions to estimate dry soil layers along an 860-km long transect on China's Loess Plateau, Geoderma, 369, 114320, 2020.

https://doi.org/10.5194/essd-2026-437
Preprint. Discussion started: 11 August 2026

Zhao, C., Jia, X., Shao, M. A., and Zhu, Y.: Regional variations in plant-available soil water storage and related driving factors in the middle reaches of the Yellow River Basin, China, Agric. Water Manage., 257, 107131, 2021.

Zhao, C., Shao, M. A., Jia, X., and Zhu, Y.: Estimation of spatial variability of soil water storage along the south–north transect on China's Loess Plateau using the state-space approach, J. Soils Sediments, 17, 1009–1020, 2017a.

Zhao, C., Shao, M. A., Jia, X., Huang, L., and Zhu, Y.: Spatial distribution of water-active soil layer along the south-north transect in the Loess Plateau of China, J. Arid Land, 11, 228–240, 2019a.

Zhao, W., Jia, X., Hu, W., Li, X., Zhao, C., Gao, L., Jia, Y., and Shao, M.: A dataset of soil water measurements at multiple scales and depths on China's Loess Plateau [Data set], https://zenodo.org/records/21859310, 2026.

Zhu, Y. J., Jia, X. X., and Shao, M. A.: Loess Thickness Variations Across the Loess Plateau of China, Surv. Geophys., 39, 715–727, 2018.

Zhu, Y. J., Jia, X. X., Qiao, J. B., Binley, A., Horton, R., Hu, W., Wang, Y. Q., and Shao, M. A.: Capacity and distribution of water stored in the vadose zone of the Chinese Loess Plateau, Vadose Zone J., 18(1), 180203, 2019.

Zreda, M., Desilets, D., Ferré, T. P. A., and Scott, R. L.: Measuring soil moisture content non-invasively at intermediate spatial scale using cosmic-ray neutrons, Geophys. Res. Lett., 35(21), 2008.